Synchronization, Channel Estimation, and Equalization in MB-OFDM Systems

Y. Li, *Student Member, IEEE*, H. Minn, *Senior Member, IEEE*, and R. M. A. P. Rajatheva, *Senior Member, IEEE*

***Abstract*— This paper addresses preamble-based low complexity synchronization, channel estimation and equalization for Zero-padded (ZP) MB-OFDM based UWB systems. The proposed synchronization method consists of sync detection, coarse timing estimation, fine timing estimation, and oscillator frequency offset estimation. The distinctive features of MB-OFDM systems and the interplay between the timing and carrier frequency hopping at the receiver are judiciously incorporated in the proposed synchronization method. In order to apply the low complexity one-tap frequency-domain equalizer, the required circular convolution property of the received signal is obtained by means of an overlap-add method after the frequency offset compensation. The proposed low complexity channel estimator for each band is developed by first averaging the over-lap-added received preamble symbols within the same band and then applying time-domain least-squares method followed by the discrete Fourier transform. We develop an MMSE equalizer and its approximate version with low complexity. We also derive the probability density functions of the UWB channel path delays, and using them we present several optimization criteria for our proposed synchronization, channel estimation, and equalization. The effectiveness of our proposed methods and optimization criteria are confirmed by computer simulation results.**

***Index Terms*— BLUE, channel estimation, equalization, frequency offset, OFDM, synchronization, timing offset, UWB.**

I. Introduction

ONE of the promising ultra-wide band (UWB) technologies is multi-band orthogonal frequency division multiplexing (MB-OFDM) [1] which has been proposed for the IEEE 802.15.3a and ECMA standard [2] [3]. OFDM is a relatively mature technology and has been adopted in digital broadcasting, wireless LAN and MAN standards. OFDM has several advantages such as low complexity equalization in dispersive channels and the spectral scalability/adaptability. However, OFDM is more susceptible to nonlinear distortion at the transmit power amplifier [4] and more sensitive to synchronization errors [5] [6]. It is shown in [7] that the MB-OFDM based UWB receivers are quite sensitive to carrier frequency estimation errors. Hence, the application of OFDM technology in UWB systems requires a high performance synchronization method, while UWB systems demand a low complexity approach.

The MB-OFDM systems from [2] [3] have the following distinctive characteristics if compared to conventional OFDM systems: 1) different channel responses and channel energies across different bands, 2) different carrier frequency offsets across different bands, 3) the use of zero padding (ZP) instead of cyclic prefix (CP), 4) the interplay between the timing and the frequency hopping (a mismatched timing point at the receiver will yield a mismatched frequency hopping and hence a significant performance degradation). These characteristics provide diversity components as well as additional design constraints, and hence, should be taken into account in the designs of synchronization, channel estimation, and equalization.

There exist several preamble-based synchronization and channel estimation methods for regular OFDM systems (e.g., see [8]–[11] and references therein), but only a few counterparts for MB-OFDM-based UWB systems [12]–[15]. These existing works have overlooked most of the distinctive features of MB-OFDM systems. The works in [13] and [14] applied the concept of utilizing the first significant channel tap for timing improvement, which was previously proposed in [10] [11] for regular OFDM systems, in MB-OFDM systems. [13] considered a ZP MB-OFDM system with the same frequency offset and channel impulse response for all bands, while [14] considered a CP MB-OFDM system with independent channels across different bands and no frequency offset. The work in [12] developed best linear unbiased estimation (BLUE) based oscillator frequency offset (OFO) estimators for MB-OFDM systems by exploiting some of the MB-OFDM characteristics, but other synchronization, channel estimation and equalization tasks were not addressed and the interplay between the timing and the frequency hopping was not considered. An MMSE-based one-tap equalizer for ZP MB-OFDM systems was recently proposed in [15], but no optimization for ZP MB-OFDM systems was attempted, and the method is, as will be shown in this paper, just an approximate MMSE. The overlap-add (OLA) method was proposed in [16] for the low complexity equalization in ZP OFDM systems, but the effects of OLA window lengths and timing offsets were not considered.

In this paper, we propose low-complexity synchronization, channel estimation and equalization methods and corresponding parameter optimizations for ZP MB-OFDM systems based on the preamble of [2] [3]. The main contributions of this paper are as follows.

1) We derive the probability density functions (pdf) and the

Manuscript received June 5, 2007; revised September 23, 2007; accepted November 6, 2007. The associate editor coordinating the review of this paper and approving it for publication was E. Serpedin. This paper was presented in parts at ICC 2007.

Y. Li and H. Minn are with the Department of Electrical Engineering, University of Texas at Dallas, P.O. Box 830688, EC 33, Richardson, TX 75080 USA (e-mail: {yxl044000, hlaing.minn}@utdallas.edu).

R. M. A. P. Rajatheva is with the Asian Institute of Technology, PO Box 4, Klong Luang 12120, Pathumthani, Thailand (e-mail: rajath@ait.ac.th).

The work of H. Minn was supported by the Erik Jonsson School Research Excellence Initiative, the University of Texas at Dallas, USA.

Digital Object Identifier 10.1109/T-WC.2008.070601

statistics of the channel path delays of the IEEE 802.15 UWB channel model from [17]. Note that these pdfs are also useful in evaluating or optimizing the energy capture of other UWB systems.

2) We present distinctive characteristics of the ZP MB-OFDM systems which are worthy to be taken into account into the system design but have been overlooked by the existing works.
3) We present how to optimize the parameter settings of the proposed synchronization, channel estimation, and equalization methods by utilizing the distinctive characteristics of the ZP MB-OFDM systems and the channel path delay pdfs we derive. Note that existing works neither exploited all of these characteristics nor addressed all synchronization, channel estimation and equalization tasks together.
4) We derive an exact MMSE equalizer for ZP MB-OFDM systems, and its low-complexity implementation. Our MMSE equalizer reduces to the equalizer in [15] after a high SNR approximation.
5) Our investigation provides new insights for improving the receiver functionalities with low complexity. For example, it reveals different performance sensitivities to different parameters, and provides guidelines in setting these parameters for robustness and complexity-reduction.

The rest of this paper is organized as follows. Section II describes the signal and channel models. Section III introduces the statistics of the UWB channels. The proposed synchronization, channel estimation, and equalization methods are presented in Section IV, and the parameter optimizations of the proposed methods are described in Section V. Simulation results and discussions are provided in Section VI, and the paper is concluded in Section VII.

Notations: The superscripts T and H represent the transpose and the Hermitian transpose, respectively. The kth row, nth column element of a matrix $\boldsymbol{X}$ is denoted by $[\boldsymbol{X}]_{k,n}$. $E[\cdot]$ represents a statistical expectation. The $N \times N$ unitary DFT matrix is denoted by $\boldsymbol{F} = [\boldsymbol{f}_0, \boldsymbol{f}_1, \ldots, \boldsymbol{f}_{N-1}]$, while $\boldsymbol{F}_K$ is the sub-matrix of $\boldsymbol{F}$ consisting of the first K columns and $\boldsymbol{F}(:, i:k)$ represents $[\boldsymbol{f}_i, \boldsymbol{f}_{i+1}, \ldots, \boldsymbol{f}_k]$. The corresponding frequency-domain variable of a time domain variable x is denoted by $\tilde{x}$. $\Re\{\cdot\}$ represents the real part of $\{\cdot\}$. The $N \times N$ identity matrix is denoted by $\boldsymbol{I}$ and $\boldsymbol{e}_i$ represents the ith column of $\boldsymbol{I}$.

II. Signal and Channel Models

We consider the MB-OFDM-based UWB systems from [2] [3] where the carrier frequency is hopped within a predefined set of carrier frequencies $\{f_q\}$ (corresponding to disjoint frequency bands) from symbol to symbol, according to a time-frequency code. The MB-OFDM system from [2] and [3] has 4 different preamble patterns (for 4 pico-nets), each associated with a different time-frequency code. Each preamble pattern is constructed by a synchronization sequence portion followed by a channel estimation sequence portion. The synchronization sequence is composed by successively repeating a time-domain preamble sequence (symbol) over 24 periods with an inverted polarity for the last period in each band. The channel estimation sequence is composed of 6 identical periods of the frequency-domain channel estimation sequence. The structures of the preamble pattern 1 in each of the three different bands are shown in Fig. 1 (see [3] [12] for other patterns).

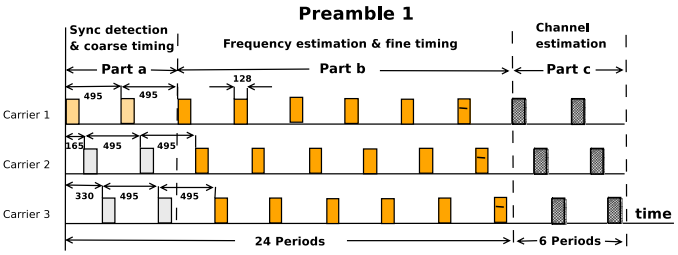

Fig. 1. The structure of the preamble pattern 1 from [2] and [3] (Also shown are the three preamble parts used in our synchronization method. The preamble symbols of carrier 2 and 3 within Part-a are not used in our synchronization method.

The MB-OFDM-based systems from [2] and [3] use ZP guard intervals consisting of $N_{\rm pre}$ prefix and $N_{\rm suf}$ suffix zero samples, instead of the conventional CP guard interval. An OFDM symbol including the guard interval has a total of $M = N + N_g$ samples where $N_g = N_{\rm pre} + N_{\rm suf}$ and, N is the number of the OFDM sub-carriers. Between ith and $(i+1)$th OFDM symbols in [2] and [3], there are 37 guard samples consisting of $N_{\rm suf} = 32$ suffice samples and $N_{\rm pre} = 5$ prefix samples. The preamble sample index 0 corresponds to the first non-zero sample of the first preamble symbol. Denote the low-pass-equivalent time-domain samples (sampled at $N/T = 1/T_s$, N times the sub-carrier spacing) transmitted in the q-th frequency band by $\{s_q(k)\}$ and their corresponding frequency-domain symbols by $\{\tilde{s}_q(n)\}$. During the m-th symbol interval, i.e., $k \in [mM - N_{\rm pre}, (m+1)M - N_{\rm pre} - 1]$, $\{s_q(k)\}$ can be all zeros if no signal is transmitted in the qth band.

The IEEE 802.15.3a UWB RF channel model described in [17] is given by

$$h_{\rm RF}(t) = X \sum_{l=0}^{L_h} \sum_{k=0}^{K} \alpha_{k,l} \delta(t - T_l - \tau_{k,l}) \qquad (1)$$

where T_l, $\tau_{k,l}$, and X are random variables representing the delay of the l-th cluster, the delay (relative to the l-th cluster arrival time) of the k-th multipath component of the l-th cluster, and the log-normal shadowing, respectively. The channel coefficients are defined as a product of small-scale and large-scale fading coefficients, i.e., $\alpha_{k,l} = p_{k,l}\xi_l\beta_{k,l}$ where $p_{k,l}$ takes on equiprobable ± 1 to account for signal inversion due to reflections, and $\{\xi_l\beta_{k,l}\}$ are log-normal distributed path gains. Then we have $E\left[\alpha_{k,l}(T_l, \tau_{k,l})\right] = 0$ and $E\left[|\alpha_{k,l}(T_l, \tau_{k,l})|^2\right] = \Omega_0 e^{-T_l/\Gamma} e^{-\tau_{k,l}/\gamma}$. Γ and γ are the cluster decay factor and ray decay factor, respectively. Details of the channel models are referred to [17].

In this paper, we consider a low-pass-equivalent system that absorbs the carrier-frequency hopping into the channel impulse response (CIR). The sample-spaced low-pass-equivalent CIR

for the q-th band is given by

$$h_q(n) = X \sum_{l=0}^{L_h} \sum_{k=0}^{K} \alpha_{k,l} e^{-j2\pi f_q(T_l+\tau_{k,l})} p(nT_s - T_l - \tau_{k,l} - t_0) \tag{2}$$

where the effect of the combined transmit and receive filter with the impulse response $p(t)$ whose span is $[-t_0, t_0]$ has been included in the CIR, and the delay t_0 is inserted for the causality.

Define $\{t_l^q\} = \{t_l^q(i) : \ i = 0, \ldots, N'-1; l = 1, \ldots, L_q\}$ where $\{t_l^q(i) : i = 0, 1, \ldots, N'-1\}$ denotes the time-domain sample index set corresponding to the l-th non-zero preamble symbol period in the q-th band with $N \le N' \le N + N_{\text{suf}}$. L_q is the number of nonzero preamble symbols in the q-th band and depends on the preamble pattern and the band index q. Let $\{x_q(k)\}$ denote the low-pass-equivalent time-domain channel output signal samples corresponding to the q-th band. Then the corresponding low-pass-equivalent time-domain received samples $\{\bar{r}_q(t_l^q(i))\}$ in the q-th band can be expressed as [1]

$$\bar{r}_q(t_l^q(i)) = e^{j2\pi \upsilon_q t_l^q(i)/N} x_q(t_l^q(i)) + n(t_l^q(i)) \tag{3}$$

where $\{n(t_l^q(i))\}$ are zero-mean independent and identically-distributed circularly-symmetric complex Gaussian noise samples with variance $\sigma^2 = E\{|n(t_l^q(i))|^2\}$, and υ_q is the normalized (by the subcarrier spacing) carrier frequency offset (CFO) of the q-th band which is related to the normalized OFO υ by

$$\upsilon_q = b_q \ \upsilon, \quad \text{for} \quad q = 1, 2, 3. \tag{4}$$

For the frequency synthesizer in [1], we have $[b_1, \ b_2, \ b_3] = \left[\frac{13}{16}, \ \frac{15}{16}, \ \frac{17}{16}\right]$ (c.f. [12]). Since the receiver does not know in advance when the preamble will arrive, we denote the low-pass-equivalent received signal as $\{r_q(k)\}$ which contains noise-only samples followed by the received preamble samples $\{\bar{r}_q(m)\}$. The number of the initial noise-only samples is a random variable depending on the arrival time of the preamble and the receiver's sync detection window timing.

III. Statistics of the UWB Channel Models

We first derive the pdf of the delay $Z_{k,l} \triangleq T_l + \tau_{k,l}$ for the k-th ray of the l-th cluster of the UWB channel, from which the pdfs of T_l and $\tau_{k,l}$ are obtained.

Note that $T_0 = 0$, $\tau_{0,l} = 0$; and $Z_{k,l}$ can be expressed as the sum of inter-arrival times of the first l clusters and the first k rays of the lth cluster. Since inter-arrival times of the UWB channel paths are independent exponential random variables, $Z_{k,l}$ is the sum of $(l+k-2)$ independent exponential random variables. The moment generating function of $Z_{k,l}$ is given by

$$\Phi_{Z_{k,l}}(s) = \left(\frac{\Lambda}{\Lambda - s}\right)^l \left(\frac{\lambda}{\lambda - s}\right)^k, \ \forall k, l \ \text{ except } k = l = 0. \tag{5}$$

[1]An arbitrary carrier phase offset can be absorbed into the CIR and hence it is not included explicitly in the signal model.

Λ and λ are the cluster arrival rate and the ray arrival rate, respectively. The m-th moment of $Z_{k,l}$ is obtained as

$$\begin{aligned} E[z_{k,l}^m] &= \frac{d^m \Phi_{Z_{k,l}}(s)}{ds^m}|_{s=0} \\ &= \sum_{i=0}^{m} \binom{m}{i} \prod_{n=0}^{i-1} (-l-n)(-\Lambda)^{-i} \prod_{u=0}^{m-i-1} (-k-u)(-\lambda)^{-m+i}. \end{aligned} \tag{6}$$

Applying the residue theory, we obtain the pdf of $Z_{k,l}$ as

$$\begin{aligned} f_{Z_{k,l}}(z_{k,l}) &= \int_{-\infty}^{\infty} \Phi_{Z_{k,l}}(s) e^{-s z_{k,l}} ds \\ &= \begin{cases} (R_1 + R_2)\Lambda^l \lambda^k (-1)^{(l+k)} & k \neq 0 \text{ or } l \neq 0 \\ \delta(z_{k,l}) & k = 0 \ \& \ l = 0 \end{cases} \end{aligned} \tag{7}$$

where

$$R_1 = \begin{cases} (-1)^l e^{-\Lambda z_{k,l}} \sum_{i=0}^{l-1} \frac{\prod_{m=0}^{i-1}(k+m)}{i!(l-i-1)!} & \\ \quad (\Lambda - \lambda)^{(-k-i)} z_{k,l}^{(l-i-1)} u(z_{k,l}) & k \neq 0 \ \& \ l \neq 0 \\ \frac{(-1)^l}{(l-1)!} z_{k,l}^{(l-1)} e^{-\Lambda z_{k,l}} u(z_{k,l}) & k = 0 \ \& \ l \neq 0 \\ 0 & l = 0 \end{cases}$$

$$R_2 = \begin{cases} (-1)^k e^{-\lambda z_{k,l}} \sum_{i=0}^{k-1} \frac{\prod_{m=0}^{i-1}(l+m)}{i!(k-i-1)!} & \\ \quad (\Lambda - \lambda)^{(-l-i)} z_{k,l}^{(k-i-1)} u(z_{k,l}) & k \neq 0 \ \& \ l \neq 0 \\ \frac{(-1)^k}{(l-1)!} z_{k,l}^{(k-1)} e^{-\lambda z_{k,l}} u(z_{k,l}) & k \neq 0 \ \& \ l = 0 \\ 0 & k = 0, \end{cases}$$

with $u(\cdot)$ being the unit step function.

Since $\{T_l\}$ and $\{\tau_{k,l}\}$ are independent, we have

$$f_{T_l, \tau_{k,l}}(x, y) = f_{t_l}(x) f_{\tau_{k,l}}(y) \tag{8}$$

where $f_{T_l}(x) = f_{Z_{0,l}}(x)$ and $f_{\tau_{k,l}}(y) = f_{Z_{k,0}}(y)$.

Next, we find the covariance matrix of the CIR for each band. Let L denote the maximum length of the sample-spaced CIR vector of each band and $\boldsymbol{h}_q$ denote the $L \times 1$ CIR vector of the qth band. Depending on the actual length of each channel realization, $\boldsymbol{h}_q$ may contain some zero samples. The covariance matrices of $\boldsymbol{h}_q$ are the same for all bands as will be apparent in the following. Hence, we simply denote the covariance matrix of $\boldsymbol{h}_q$ by $\boldsymbol{C}_h$. From (2), we can calculate the element of $\boldsymbol{C}_h$ as[2]

$$\begin{aligned} C_h(m,n) = \int_0^{\infty} \int_0^{\infty} \sum_{l=0}^{L_h} \sum_{k=0}^{K} & E\left[|\alpha_{k,l}(T_l, \tau_{k,l})|^2\right] \\ & \times p(mT_s - T_l - \tau_{k,l} - t_0) p(nT_s - T_l - \tau_{k,l} - t_0) \\ & \times f_{T_l, \tau_{k,l}}(T_l, \tau_{k,l}) \ dT_l \ d\tau_{k,l} \end{aligned} \tag{9}$$

where we have used the statistical independence among $\{\alpha_{k,l}(T_l, \tau_{k,l})\}$.

Substituting (7)-(8) and $E\left[|\alpha_{k,l}(T_l, \tau_{k,l})|^2\right] = \Omega_0 e^{-T_l/\Gamma} e^{-\tau_{k,l}/\gamma}$ into (9) gives

$$\begin{aligned} C_h(m,n) = \sum_{l=0}^{L_h} \sum_{k=0}^{K} \int_0^T \int_0^T & \Omega_0 e^{-T_l/\Gamma} e^{-\tau_{k,l}/\gamma} \\ & \times p(mT_s - T_l - \tau_{k,l} - t_0) \ p(nT_s - T_l - \tau_{k,l} - t_0) \\ & \times f_{Z_{0,l}}(T_l) f_{Z_{k,0}}(\tau_{k,l}) \ dT_l \ d\tau_{k,l} \end{aligned} \tag{10}$$

[2]We neglect the shadowing parameter X in this paper and hence realizations of $\{\alpha_{k,l}\}$ are not normalized.

which can be numerically evaluated. We will use the above channel covariance matrix in optimizing our proposed methods in Section V. Note that the pdfs of the UWB channel path delays we derive are also useful in calculating or optimizing the energy capture of other UWB systems.

IV. Proposed Synchronization, Channel estimation and Equalization

In this paper, we consider sync detection, timing offset estimation, OFO estimation, channel estimation and equalization for the packet-based MB-OFDM system in [2] and [3]. We assume that the receiver knows what preamble the transmitter uses but not the OFO and the arrival time of the preamble.

The whole interval of the 30 preamble symbols with the sample index set $\{t_l^q(i)\}$ is divided into three disjoint parts – part-*a*, part-*b*, and part-*c* – with the corresponding sample index sets $\{t_{a,l}^q(i)\}$, $\{t_{b,l}^q(i)\}$, and $\{t_{c,l}^q(i)\}$, respectively. All the distances of the preamble symbol pairs within part-x are denoted by $\{d_x(m) : m = 1, 2, \ldots\}$ where x is *a*, *b*, or *c* representing the corresponding part. For example, for the preamble pattern 1, we may set the first part as the first 6 symbol interval, the second part as the next 18 symbol interval, and the third part as the last 6 symbol interval (see Fig. 1). In this case, $\{t_{a,l}^q(i)\} = \{t_l^q(i) : l = 1, 2\}$, $\{t_{b,l}^q(i)\} = \{t_l^q(i) : l = 3, 4, 5, 6, 7, 8\}$, $\{t_{c,l}^q(i)\} = \{t_l^q(i) : l = 9, 10\}$, $\{d_b(m)\} = \{3M, 6M, 9M, 12M, 15M\}$. We also define $d_x(0) = 0$ for convenience.

Define the correlation term with a correlation distance $d_x(m)$ between non-zero received preamble symbols within part-x in the q-th band as

$$R_{x,q}(m, k_{\rm t}, N') = \sum_{\substack{\{k,\, k+d_x(m)\} \\ \in \{k_{\rm t} + t_{x,l}^q(i)\}}} (-1)^{\epsilon}\, r_q^*(k) r_q(k + d_x(m)) \quad (11)$$

where

$$\epsilon = \begin{cases} 1, & \text{if } \{k + d_x(m)\} \in \{k_{\rm t} + t_{b,8}^q(i)\} \\ 0, & \text{else} \end{cases} \quad (12)$$

note that $i = 0, 1, \ldots, N' - 1$. ϵ is a parameter introduced by the burst cover sequence (see [2] [3] for details). During part-*a* where the sync detection and coarse timing estimation are performed, the receiver carrier frequency hopping is not performed. During the remaining parts, the receiver carrier frequency is hopped according to the preamble pattern. The fine timing and the OFO estimations are based on the received preamble symbols within part-*b*, while channel estimation task is based on part-*c* [3]. The reason for the use of only part-*b* for the fine timing estimation is to allow processing time so that timing adjustment (for frequency hopping instants) based on the fine timing estimation can be made at the end of the preamble. The receiver tasks are performed in the following order: sync detection, coarse timing estimation, fine timing estimation, OFO estimation and compensation, channel estimation, equalization and data detection.

[3]Note that preamble symbols from part-*b* can also be used to improve the channel estimation.

A. Sync Detection and Coarse Timing Estimation

The carrier frequency of the receiver is initially set to the one that corresponds to the first preamble symbol, and denote the corresponding band index by $\bar{q}$. During the sync detection process, the receiver carrier frequency hopping is not performed since it requires timing information which is unavailable yet. We use the first two preamble symbols in the $\bar{q}$th band to detect the arrival of the preamble. Then the sync detection metric is given by

$$\mathcal{M}(k) = |R_{a,\bar{q}}(1, k, N')|\,. \quad (13)$$

For complexity reduction[4] and energy saving, the computation of $\mathcal{M}(k)$ is performed only at $k = 0$, Δ, 2Δ, ..., where Δ (an integer) is a design parameter.

Once $\mathcal{M}(k)$ becomes larger than a pre-defined threshold $\mathcal{M}_{\rm SD}$, say at $k = k_{\rm SD}$, the receiver decides that the preamble has been detected and starts finding the coarse timing point as follows:

$$k_{\rm ct} = \underset{k_{\rm SD} \le k \le k_{\rm SD} + W_1 - 1}{\arg\max} \{\mathcal{M}(k)\} \quad (14)$$

where W_1 is the length of the window within which the coarse timing point is searched and W_1 can be set to M. A lower complexity version of the above coarse timing estimator can be implemented by finding the point k_1 corresponding to the maximum of the metric values at $k = k_{\rm SD}$, $k_{\rm SD} + \Delta_1$, $k_{\rm SD} + 2\Delta_1$, ... , and then the point corresponding to the maximum of the metric values at $k_1 - \lceil \Delta_1/2 \rceil$, $k_1 - \lceil \Delta_1/2 \rceil + 1$, ..., $k_1 + \lceil \Delta_1/2 \rceil$. Here, Δ_1 (an integer) is a design parameter. Based on the coarse timing point $k_{\rm ct}$, the receiver determines at what time instant it should hop the carrier frequency to demodulate the rest of the preamble.

B. Fine Timing Offset Estimation

The fine timing estimation is based on the preamble part-*b* while the coarse timing estimation is based on part-*a*. Hence, the correct points for the coarse timing point $k_{\rm ct}$ and the fine timing point $k_{\rm ft}$ correspond to the beginning of part-*a* and part-*b*, respectively. We denote the beginning of part-*b* by $k_{\rm ref}$. The proposed fine timing estimator is described by [5]

$$k_{\rm ft} = -\eta + \underset{i \in (k_{\rm ct} + D_a - W_2,\ k_{\rm ct} + D_a + W_3)}{\arg\max} \sum_{q=1}^{3} |R_{b,q}(1, i, N')| \quad (15)$$

where D_a is the length (in samples) of part-*a* and η is a fixed timing adjustment. For CP-based OFDM systems, η should be set such that the timing point is most of the time within the ISI-free part of the CP [10]. We will describe how to set η for the considered ZP OFDM system in Section VI.

C. OFO Estimation and Compensation

We adopt the BLUE-based OFO estimator from [12] with a few differences. In [12] the OFO estimator utilizes the first 21 preamble symbols, while in this paper the OFO estimator

[4]$\mathcal{M}^2(k)$ can also be used in place of $\mathcal{M}(k)$.

[5]Note that although more correlation terms can be included in the fine timing estimation, for low complexity implementation we just use the correlation terms with the correlation distance $d_b(1)$.

is based only on part-*b* allowing processing time and resource for prior tasks of sync detection and coarse timing estimation. Furthermore, the correlation window length for each preamble symbol is fixed at N samples in [12] but is set to N' in this paper which will be optimized for better performance.

The OFO estimator is given by

$$\widehat{\upsilon} = \frac{\sum_{q=1}^{3} \mathbf{1}^T \boldsymbol{C}_{\theta_q}^{-1} \mathbf{1}\ b_q \widehat{\upsilon}_q}{\sum_{q=1}^{3} \mathbf{1}^T \boldsymbol{C}_{\theta_q}^{-1} \mathbf{1}\ b_q^2} \tag{16}$$

where

$$\widehat{\upsilon}_q = \sum_{m=1}^{H_q} \omega_q(m)\theta_q(m) \tag{17}$$

$$\theta_q(m) = \frac{N}{2\pi d_{\rm b}(m)} \text{angle}\{R_{b,q}(m, k_{\rm ft}, N')\} \tag{18}$$

with $\omega_q(m)$ being the m-th component of the weighting vector

$$\boldsymbol{\omega}_q = \boldsymbol{C}_{\theta_q}^{-1}\mathbf{1}\left(\mathbf{1}^T\boldsymbol{C}_{\theta_q}^{-1}\mathbf{1}\right)^{-1}. \tag{19}$$

In (19), $\boldsymbol{C}_{\theta_q}$ is the covariance matrix of $\{\theta_q(m) : m = 1, \ldots, H_q\}$, H_q is a design parameter (see [12]) and $\mathbf{1}$ denotes the all-one column vector, whose size should be apparent from the expression. Two approaches (Methods A and B) for the calculation of $\{\boldsymbol{C}_{\theta_q}\}$ are given in [12]. Due to the different window length in this paper, the covariance matrices $\{\boldsymbol{C}_{\theta_q}\}$ become slightly different from those in [12]. For example, for preamble pattern 1 or 2, denoting the number of non-zero preamble symbols within the combined part-*b* in the qth band by $\bar{L}_q$, and applying Method A, we obtain

$$\boldsymbol{C}_{\theta_q}(m,n) = g(m,n) \times \begin{cases} m + \frac{(\bar{L}_q - m)N'\sigma^2}{2E_{x,q}(N')}, & \text{if } m = n \ \&\ m < \bar{L}_q/2 \\ (\bar{L}_q - m) + \frac{(\bar{L}_q - m)N'\sigma^2}{2E_{x,q}(N')}, & \text{if } m = n \ \&\ m \geq \bar{L}_q/2 \\ \min(m,n), & \text{if } m \neq n \ \&\ m + n < \bar{L}_q \\ \bar{L}_q - \max(m,n), & \text{if } m \neq n \ \&\ m + n \geq \bar{L}_q \end{cases} \tag{20}$$

where

$$g(m,n) = \frac{N^2\sigma^2}{4\pi^2(3M)^2 E_{x,q}(N')} \frac{1}{mn(\bar{L}_q - m)(\bar{L}_q - n)} \tag{21}$$

and applying Method B gives

$$\boldsymbol{C}_{\theta_q}(m,n) = g(m,n) \times \begin{cases} \min(m,n), & \text{if } \ m + n < \bar{L}_q \\ \bar{L}_q - \max(m,n), & \text{if } \ m + n \geq \bar{L}_q. \end{cases} \tag{22}$$

The estimator in (16) can be implemented as

$$\widehat{\upsilon} = \frac{\sum_{q=1}^{3} \widehat{E}_{x,q}(N') A_q b_q \widehat{\upsilon}_q}{\sum_{q=1}^{3} \widehat{E}_{x,q}(N') A_q b_q^2} \tag{23}$$

where the received preamble symbol energy estimate in the qth band is calculated as

$$\widehat{E}_{x,q}(N') = R_{b,q}(0, k_{\rm ft}, N')/\bar{L}_q, \tag{24}$$

and A_q can be pre-computed as

$$A_q = \frac{\mathbf{1}^T\boldsymbol{C}_{\theta_q}^{-1}\mathbf{1}}{E_{x,q}(N')}. \tag{25}$$

Next, CFO compensation for the qth band is performed starting from preamble part-*b* as

$$r_q(k_{\rm ft} + m)e^{-j2\pi m\widehat{\upsilon} b_q/N} \triangleq \check{\mathrm{r}}_q(k_{\rm ft} + m) \text{ for } m = 0, 1, \ldots. \tag{26}$$

D. Channel Estimation

The use of zero-amplitude guard samples in MB-OFDM UWB systems [2] [3] instead of conventional CP guard samples saves transmit power and allows a sufficient amount of time for the transmitter and receiver to switch between carrier frequencies. To obtain the circular convolution property required for the frequency-domain one-tap equalization, we apply the OLA method [16] to the frequency-offset-compensated received signal. Specifically, for every l-th non-zero OFDM symbol in the qth band after CFO compensation, the OLA method adds $M_0 (0 \leq M_0 \leq N_{\rm suf})$ samples $\{\check{\mathrm{r}}_q(k_{\rm ft} + lM + N), \check{\mathrm{r}}_q(k_{\rm ft} + lM + N + 1), \ldots, \check{\mathrm{r}}_q(k_{\rm ft} + lM + M_0 + N - 1)\}$ to $\{\check{\mathrm{r}}_q(k_{\rm ft} + lM), \check{\mathrm{r}}_q(k_{\rm ft} + lM + 1), \ldots, \check{\mathrm{r}}_q(k_{\rm ft} + lM + M_0 - 1)\}$, resulting in an $N \times 1$ vector $\boldsymbol{y}_q^{(l)}$ with the k-th element given by

$$y_q^{(l)}(k) = \begin{cases} \check{\mathrm{r}}_q(k_{\rm ft} + lM + k) \\ \quad + \check{\mathrm{r}}_q(k_{\rm ft} + lM + k + N), & \text{if } \ 0 \leq k \leq M_0 - 1 \\ \check{\mathrm{r}}_q(k_{\rm ft} + lM + k), & \text{else.} \end{cases} \tag{27}$$

The OLA length M_0 need not be the same for preamble symbol and data symbol. We use M_p and M_d to denote the OLA length for preamble symbol and data symbol, respectively.

After applying the OLA method, the preamble symbols in each band are averaged as

$$\bar{\boldsymbol{y}}_q = \frac{1}{L_{q,\rm c}} \sum_{l=1}^{L_{q,\rm c}} \boldsymbol{y}_q^{(l)} \tag{28}$$

where $L_{q,\rm c}$ is the number of non-zero preamble symbols of part-*c* in the qth band. After applying CFO compensation and the OLA method, we can assume in developing the CIR estimator that $\bar{\boldsymbol{y}}_q$ is approximately the same as the received preamble symbol with circular convolution property under perfect frequency synchronization but with a possible timing offset. Although the maximum number of CIR taps is L, we estimate length-L' CIR to account for the effects of random timing offset on the channel estimation. The optimization of L' will be discussed in Section V-C. We apply the time-domain least-squares channel estimator and obtain the length L' CIR vector estimate for the qth band as

$$\hat{\boldsymbol{h}}_q = (\boldsymbol{S}^H\boldsymbol{S})^{-1}\boldsymbol{S}^H\bar{\boldsymbol{y}}_q \tag{29}$$

where $[\boldsymbol{S}]_{k,n} = s((k - n) \bmod N)$, $0 \leq k \leq N - 1$, $0 \leq n \leq L' - 1$, and $\{s(m) : m = 0, 1, \ldots, N - 1\}$[6] are the low-pass-equivalent time-domain OFDM preamble samples. Further improvements on the channel estimation and timing estimation (e.g., see [10] [11]) are possible at the cost of much larger complexity, but we will not pursue them here since UWB systems demand low complexity algorithms. The frequency-domain channel estimates are then simply obtained

[6]The band index q is dropped since the preamble symbols are the same.

by taking the DFT of $\hat{\boldsymbol{h}}_q$ as $[\tilde{\hat{h}}_q(0), \tilde{\hat{h}}_q(1), \ldots, \tilde{\hat{h}}_q(N-1)]^T = \sqrt{N}\boldsymbol{F}_{L'}\hat{\boldsymbol{h}}_q$.

E. Equalization

1) One-tap Zero-Forcing (ZF) Equalizer: In general, data can be transmitted with or without spreading using a time-frequency code. Suppose the mth OFDM data symbol (after spreading if applied) is transmitted in the qth band, and let $\tilde{y}_{q,m}(i)$ denote the corresponding received symbol on the ith subcarrier after performing CFO compensation, the OLA method, and DFT. If the data are not spread by a time-frequency code, the frequency-domain one-tap ZF equalizer output decision variable for the ith subcarrier data of the mth OFDM data symbol is given by

$$\tilde{Y}^{(m)}(i) = \tilde{\hat{h}}_q(i)^* \tilde{y}_{q,m}(i) / |\tilde{\hat{h}}_q(i)|^2. \tag{30}$$

If data spreading is performed using a time-frequency code [2] [3] such as each data symbol is transmitted on two consecutive symbol intervals using a frequency hopping pattern of [l_0 n_0 l_1 n_1 l_2 n_2] (e.g., [1 2 3 1 2 3]), then the ZF equalizer output decision variable for the mth data (before spreading) on the i-th subcarrier is obtained as

$$\tilde{Y}^{(m)}(i) = \frac{\left(\tilde{\hat{h}}_{l_\xi}(i)^* \tilde{y}_{l_\xi,2m}(i) + \tilde{\hat{h}}_{n_\xi}(i)^* \tilde{y}_{n_\xi,2m+1}(i)\right)}{\left(|\tilde{\hat{h}}_{l_\xi}(i)|^2 + |\tilde{\hat{h}}_{n_\xi}(i)|^2\right)} \tag{31}$$

where $\xi = m \bmod 3$ in the band indexes l_ξ and n_ξ.

2) MMSE Equalizer: A one-tap MMSE-based equalizer for MB-OFDM systems has been proposed in [15] by assuming that the frequency-domain noise remains white after applying the OLA method. However, the covariance matrix of the frequency-domain noise after applying the OLA method is given by $\boldsymbol{C}_n = \sigma^2(\boldsymbol{I}_N + \boldsymbol{F}_{M_d}\boldsymbol{F}_{M_d}^H)$, which is no longer diagonal. Hence the MMSE equalizer in frequency domain is no longer a one-tap equalizer, and the equalizer proposed in [15] is not an MMSE equalizer in the strict sense. In this section, we will introduce the MMSE equalizer for the MB-OFDM systems. First we assume the data are not spread. Define

$$\boldsymbol{H}_q = \text{diag}\left\{[\tilde{\hat{h}}_q(0), \tilde{\hat{h}}_q(1), \ldots, \tilde{\hat{h}}_q(N-1)]^T\right\}. \tag{32}$$

The frequency-domain MMSE equalizer output decision variable for the mth OFDM data symbol on the qth band is given by

$$\tilde{\boldsymbol{Y}}_m = \boldsymbol{H}_q\boldsymbol{C}_{\tilde{s}}\left(\boldsymbol{H}_q\boldsymbol{C}_{\tilde{s}}\boldsymbol{H}_q^H + \boldsymbol{C}_n\right)^{-1}\tilde{\boldsymbol{y}}_{q,m} \tag{33}$$

where $\boldsymbol{C}_{\tilde{s}}$ represents the covariance matrix for transmit data in the frequency-domain. If the data are independent QPSK signals in frequency-domain, $\boldsymbol{C}_{\tilde{s}}$ is a diagonal matrix with "1"s on the transmitted subcarrier and "0"s on the guard subcarriers [2] [3].

If data are spread using a time-frequency code and the frequency hopping pattern of [l_0 n_0 l_1 n_1 l_2 n_2], the MMSE equalizer output decision variable for the mth data (before spreading) is obtained as

$$\tilde{\boldsymbol{Y}}_m = \left[\boldsymbol{H}_{l_\xi}^H\boldsymbol{C}_{\tilde{s}}\ \boldsymbol{H}_{n_\xi}^H\boldsymbol{C}_{\tilde{s}}\right]\boldsymbol{V}^{-1}[\tilde{\boldsymbol{y}}_{l_\xi,2m}^T\ \tilde{\boldsymbol{y}}_{n_\xi,2m}^T]^T \tag{34}$$

$$\text{where } \boldsymbol{V} = \begin{bmatrix}\boldsymbol{H}_{l_\xi}\boldsymbol{C}_{\tilde{s}}\boldsymbol{H}_{l_\xi}^H + \boldsymbol{C}_n & \boldsymbol{H}_{l_\xi}\boldsymbol{C}_{\tilde{s}}\boldsymbol{H}_{n_\xi}^H \\ \boldsymbol{H}_{n_\xi}\boldsymbol{C}_{\tilde{s}}\boldsymbol{H}_{l_\xi}^H & \boldsymbol{H}_{n_\xi}\boldsymbol{C}_{\tilde{s}}\boldsymbol{H}_{n_\xi}^H + \boldsymbol{C}_n\end{bmatrix} \tag{35}$$

The matrix inverse operation indicates that the MMSE equalizer is much more complicated than the one-tap ZF equalizer. We provide a much simplified computation of the inverse in (33) and (34) in Appendix.

3) One-tap MMSE Equalizer: Although the MMSE equalizer can be simplified, the complexity is still higher than the one-tap ZF equalizer. If we neglect the extra noise introduced by the OLA method, then the noise can be approximated as the white Gaussian noise with variance σ^2. Under this circumstance, the MMSE equalizers in (33) and (34) can be simplified to the same form as proposed in [15]. For the UWB system without data spreading, the output of the approximated one-tap MMSE equalizer is given by

$$\tilde{Y}^{(m)}(i) = \tilde{\hat{h}}_q(i)^* \tilde{y}_{q,m}(i) / (|\tilde{\hat{h}}_q(i)|^2 + \sigma_n^2 / E[|\tilde{s}(i)|^2]). \tag{36}$$

For the system using data spreading, the output of the approximated one-tap MMSE equalizer is given by

$$\tilde{Y}^{(m)}(i) = \frac{\left(\tilde{\hat{h}}_{l_\xi}(i)^* \tilde{y}_{l_\xi,2m}(i) + \tilde{\hat{h}}_{n_\xi}(i)^* \tilde{y}_{n_\xi,2m+1}(i)\right)}{\left(|\tilde{\hat{h}}_{l_\xi}(i)|^2 + |\tilde{\hat{h}}_{n_\xi}(i)|^2 + \sigma_n^2 / E[|\tilde{x}(i)|]^2\right)}. \tag{37}$$

Furthermore, if the frequency-domain data are QPSK symbols [2] [3], the approximated one-tap MMSE equalizer is equivalent to the one-tap ZF equalizer we introduced in (30) and (31). The reason is that the detection of QPSK symbols only depends the phase of the received signal, and the noise variance term in the expression of the approximated one-tap MMSE equalizer will not affect the received phase information.

V. Optimizing the Proposed Methods

This section presents how to optimize the proposed methods by designing the window lengths involved in several tasks. Recall that we consider $N_{\text{suf}} = 32$ zero-amplitude suffix samples and $N_{\text{pre}} = 5$ zero-amplitude prefix samples. We assume that the maximum channel dispersion is $N_{\text{suf}} = 32$ samples, and the interval of the $N_{\text{pre}} = 5$ prefix samples is reserved for switching the carrier frequency. Hence, the considered correlation window length range is $[N, N+N_{\text{suf}}] = [128, 160]$ and the OLA window length range is $[0, 32]$.

A. Window Length for Timing Estimation

Define

$$\beta(i, T_1, N') = R_{a,1}(1, T_1 + i + 1, N') - R_{a,1}(1, T_1 + i, N'). \tag{38}$$

Then for a given channel output signal $\{x_1(k)\}$, $\{\beta(i, T_1, N')\}$ are independent complex Gaussian random

$$\tilde{\boldsymbol{x}}_q^{\mathrm{ICI}} = \begin{cases} \boldsymbol{F}(:,(M_d : L-k_{\mathrm{ft}}-1))\boldsymbol{H}_a(M_d+k_{\mathrm{ft}})\left(\boldsymbol{F}(:,(N-L+M_d+k_{\mathrm{ft}} : N-1))\right)^H \tilde{\boldsymbol{s}}_q & \\ \quad + \boldsymbol{F}(:,(N-k_{\mathrm{ft}} : N-1))\boldsymbol{H}_b(k_{\mathrm{ft}})\left(\boldsymbol{F}(:,(0 : k_{\mathrm{ft}}-1))\right)^H \tilde{\boldsymbol{s}}_q & \text{if } k_{\mathrm{ft}}>0 \ \&\ M_d+k_{\mathrm{ft}}<L \\ \boldsymbol{F}(:,(N-k_{\mathrm{ft}} : N-1))\boldsymbol{H}_b(k_{\mathrm{ft}})\left(\boldsymbol{F}(:,(0 : k_{\mathrm{ft}}-1))\right)^H \tilde{\boldsymbol{s}}_q & \text{if } k_{\mathrm{ft}}>0 \ \&\ M_d+k_{\mathrm{ft}}\geq L \\ \boldsymbol{F}(:,(M_d : L-k_{\mathrm{ft}}-1))\boldsymbol{H}_a(M_d+k_{\mathrm{ft}})\left(\boldsymbol{F}(:,(N-L+M_d+k_{\mathrm{ft}} : N-1))\right)^H \tilde{\boldsymbol{s}}_q & \text{if } k_{\mathrm{ft}}\leq 0 \ \&\ M_d\geq -k_{\mathrm{ft}} \\ \boldsymbol{F}(:,(0 : L-1))\boldsymbol{H}_a(0)\left(\boldsymbol{F}(:,(N-L : N-1))\right)^H \tilde{\boldsymbol{s}}_q & \\ \quad + \boldsymbol{F}(:,(M_d : -k_{\mathrm{ft}}-1))\boldsymbol{x}_q(N+k_{\mathrm{ft}}+M_d : N-1) & \text{if } k_{\mathrm{ft}}\leq 0 \ \&\ M_d<-k_{\mathrm{ft}} \end{cases} \tag{48}$$

$$E[|\tilde{\boldsymbol{x}}_q^{\mathrm{ICI}}|^2] = \begin{cases} \mathrm{trace}\left(E[\boldsymbol{H}_a(M_d+k_{\mathrm{ft}})(\boldsymbol{H}_a(M_d+k_{\mathrm{ft}}))^H]+E[\boldsymbol{H}_b(k_{\mathrm{ft}})(\boldsymbol{H}_b(k_{\mathrm{ft}}))^H]\right) & \text{if } k_{\mathrm{ft}}>0 \ \&\ M_d+k_{\mathrm{ft}}<L \\ \mathrm{trace}\left(E[\boldsymbol{H}_b(k_{\mathrm{ft}})(\boldsymbol{H}_b(k_{\mathrm{ft}}))^H]\right) & \text{if } k_{\mathrm{ft}}>0 \ \&\ M_d+k_{\mathrm{ft}}\geq L \\ \mathrm{trace}\left(E[\boldsymbol{H}_a(M_d+k_{\mathrm{ft}})(\boldsymbol{H}_a(M_d+k_{\mathrm{ft}}))^H]\right) & \text{if } k_{\mathrm{ft}}\leq 0 \ \&\ M_d\geq -k_{\mathrm{ft}} \\ \mathrm{trace}\left(E[\boldsymbol{H}_a(0)(\boldsymbol{H}_a(0))^H]\right)-\sum_{i=N+k_{\mathrm{ft}}+M_d}^{N-1}E[|x_q(i)|^2] & \text{if } k_{\mathrm{ft}}\leq 0 \ \&\ M_d<-k_{\mathrm{ft}} \end{cases}. \tag{51}$$

variables with

$$E[\beta(i,T_1,N')] = x_1^*(i+N')x_1(i+N'+d_a(1))-x_1^*(i)x_1(i+d_a(1)) \tag{39}$$

$$\mathrm{Var}[\beta(i,T_1,N')] = \sigma^2(|x_1(i)|^2+|x_1(i+d_a(1))|^2 + |x_1(i+N')|^2+|x_1(i+N'+d_a(1))|^2)+2\sigma^4. \tag{40}$$

Then we use the following criterion to design the correlation window length N_t for timing estimation

$$N_t = \underset{N\leq N'\leq N+N_g}{\arg\max}\left\{\prod_{i=0}^{N/2}\left(1-Q\left(\frac{|E[\beta(i,T_1,N')]|}{\sqrt{\mathrm{Var}[\beta(i,T_1,N')]}}\right)\right)\right\} \tag{41}$$

where $Q(\cdot)$ is the Gaussian tail probability, and T_1 for each N' is chosen such that $[T_1, T_1+N'+N/2-1]$ is approximately symmetric with respect to $[k_{\mathrm{ref}}, k_{\mathrm{ref}}+N+N_{\mathrm{suf}}]$. This criterion can be approximately considered as the probability of the joint events $\{|R_{a,1}(1,\bar{k},N')| > |R_{a,1}(1,\bar{k}+l,N')| : l=\pm1,\pm2,\ldots\}$ where $\bar{k}$ is the time instant corresponding to the maximum of $|R_{a,1}(1,k,N')|$. In the design, we replace $|x_1(k)|^2$ with $E[|x_1(k)|^2]$ which can be calculated using the channel covariance matrix $\boldsymbol{C}_h$ obtained in Section III.

B. Window Length for OFO Estimation

We use the BLUE variance of the CFO estimation to optimize the window length for our OFO estimator. We can simply consider the BLUE variance in the qth band given by

$$\mathrm{Var}\{\widehat{\upsilon}_q|N'\} = (\mathbf{1}^T\boldsymbol{C}_{\theta_q|N'}^{-1}\mathbf{1})^{-1} \tag{42}$$

where $\boldsymbol{C}_{\theta_q|N'}$ is given in (20). Then the best window length N_f for our OFO estimator is determined by

$$N_f = \underset{N\leq N'\leq N+N_{\mathrm{suf}}}{\arg\min}\left\{\mathrm{Var}\{\widehat{\upsilon}_q|N'\}\right\}. \tag{43}$$

C. CIR Estimation Window Length and Preamble OLA Length

The channel taps with largest delays may contain negligible channel energy and neglecting them in the CIR estimation will suppress noise from those neglected taps and hence may improve the CIR estimation performance. Hence, in this section, we derive channel estimation MSE obtained with the CIR estimation window length L', and find the optimum L' which yields the minimum channel estimation MSE. Since fine timing and frequency synchronization have been performed, we develop our optimization for CIR estimation under perfect synchronization first. Next, we incorporate the effect of timing offset into our design.

After applying the OLA method with window length M_p on the CFO-compensated averaged received preamble symbol, the MSE of the length-L' CIR estimation under perfect synchronization can be derived as

$$\mathrm{MSE}_h(L',M_p) = \mathrm{trace}\left(\boldsymbol{C}_h\right)+\sigma^2\mathrm{trace}\left(\boldsymbol{\Upsilon}^H\boldsymbol{\Upsilon}(\boldsymbol{I}+\boldsymbol{T})\right) + \mathrm{trace}\left(\boldsymbol{\Upsilon}^H\boldsymbol{\Upsilon}\bar{\boldsymbol{S}}\boldsymbol{C}_h\bar{\boldsymbol{S}}\right)-2\,\Re\left\{\mathrm{trace}\left(\boldsymbol{\Upsilon}\bar{\boldsymbol{S}}\boldsymbol{C}_{\mathrm{h}}\right)\right\}. \tag{44}$$

where $\boldsymbol{T}=[\boldsymbol{e}_1,\ldots,\boldsymbol{e}_{M_p},\boldsymbol{0}_{N\times(N-M_p)}]$, $\boldsymbol{\Upsilon}=(\boldsymbol{S}^H\boldsymbol{S})^{-1}\boldsymbol{S}^H$ and $\bar{\boldsymbol{S}}=\boldsymbol{S}_L-\bar{\boldsymbol{S}}_\Delta$. $\bar{\boldsymbol{S}}_\Delta$ is an $N\times L$ matrix, and for $L>M_p$, $\bar{\boldsymbol{S}}_\Delta(M_p+1:L,M_p+1:L)=\boldsymbol{S}_\Delta$, and the other elements of $\bar{\boldsymbol{S}}_\Delta$ are all zeros. If $L\leq M_p$, $\bar{\boldsymbol{S}}_\Delta$ is the all-zero matrix. $\boldsymbol{S}_\Delta$ is an $(L-M_p)\times(L-M_p)$ matrix with the (n,k)th element given by $s(N-1-k+n)$ if $k\geq n$, and zero if $k<n$.

$\boldsymbol{S}_L$ is an $N\times L$ matrix with $[\boldsymbol{S}_L]_{k,n}=s((k-n)\bmod N)$, $0\leq k\leq N-1$, $0\leq n\leq L-1$. Then, we obtain the optimum (L',M_p) for the CIR estimation under perfect synchronization as

$$([L']^*_{\mathrm{perfect}},[M_p]^*_{\mathrm{perfect}}) = \underset{\{L',M_p\}}{\arg\min}\{\mathrm{MSE}_h(L',M_p)\} \tag{45}$$

which can be numerically evaluated where the required $\boldsymbol{C}_h(m,n)$ is obtained from (10). In the presence of timing errors, the above window lengths in (45) should be increased accordingly so that the CIR estimation window contains the first $[L']^*_{\mathrm{perfect}}$ actual channel taps most of the time. We will discuss this issue in Section VI.

D. Optimizing the Data OLA Length

The OLA method increases the noise power if compared to the CP-based systems since the noise terms are also added up. In this sense, we prefer a smaller OLA length M_d (for data) which will decrease the extra noise power. However, the shortening of the OLA length M_d may destroy the circular convolution property and in this circumstance the OLA method with one-tap frequency-domain equalizer will introduce the inter-carrier interferences (ICI). For example, with perfect timing, if M_d is less than the order of the CIR, there will be ICI. Note that the timing offset also affects the optimal value of M_d. In this section, we will find the

optimum M_d which minimizes the combined interference and extra noise power introduced by the OLA method.

After applying the OLA method, the received i-th subcarrier data can be expressed as

$$\tilde{y}_q(i) = \tilde{x}_q(i) - \tilde{x}_q^{\mathrm{ICI}}(i) + \tilde{n}_q^e(i) + \tilde{n}(i) \tag{46}$$

where $\tilde{x}_q(i) = \tilde{h}_q(i)\tilde{s}_q(i)$, $\tilde{n}(i)$ is the frequency-domain noise sample (the same statistics as in CP-based systems), $\tilde{n}_q^e(i)$ is the extra frequency-domain noise sample due to the OLA method, and $\tilde{x}_q^{\mathrm{ICI}}(i)$ is the ICI term on the i-th subcarrier due to the OLA method. Denote the corresponding vectors of $\tilde{s}_q(i)$, $\tilde{x}_q^{\mathrm{ICI}}(i)$, $\tilde{n}(i)$, and $\tilde{n}_q^e(i)$ by $\tilde{\boldsymbol{s}}_q$, $\tilde{\boldsymbol{x}}_q^{\mathrm{ICI}}$, $\tilde{\boldsymbol{n}}$, and $\tilde{\boldsymbol{n}}_q^e$, respectively. Note that we have

$$\tilde{\boldsymbol{n}}_q^e = \boldsymbol{F}(:, (0 : M_d - 1)) \times \boldsymbol{n}(k_{\mathrm{ft}} + lM + N : k_{\mathrm{ft}} + lM + N + M_d - 1). \tag{47}$$

For simplicity in presentation, we assume in this section that the perfect timing point index (for k_{ft}) is 0 (i.e., $k_{\mathrm{ref}} = 0$). Then, the ICI vector $\tilde{\boldsymbol{x}}_q^{\mathrm{ICI}}$ can be expressed as (48), where $\boldsymbol{H}_a(x)$ is an $(L-x)\times(L-x)$ matrix with the (n,k)th element being equal to $h_q(L-1-k+n)$ if $k \geq n$, and zero if $k < n$. $\boldsymbol{H}_b(x)$ is a $x \times x$ matrix with the (n,k)th element given by $h_q(n-k)$ if $n \geq k$ and zero if $n < k$.

Since we choose the same OLA length M_d for all bands and the channel covariance matrices are also the same for all bands, the interference plus extra noise power caused by the OLA method in each band can be expressed as

$$\Xi = E[|\tilde{\boldsymbol{x}}_q^{\mathrm{ICI}}|^2] + E[|\tilde{\boldsymbol{n}}_q^e|^2] \tag{49}$$

$$\text{where} \quad E[|\tilde{\boldsymbol{n}}_q^e|^2] = M_d\sigma^2. \tag{50}$$

Considering independent and identically-distributed data symbols on the subcarriers, we have $E[\tilde{\boldsymbol{s}}_q\tilde{\boldsymbol{s}}_q^H] = \sigma_s^2\boldsymbol{I}$. Then, $E[|\tilde{\boldsymbol{x}}_q^{\mathrm{ICI}}|^2]$ is given by (51). The elements of $E[\boldsymbol{H}_a(x)(\boldsymbol{H}_a(x))^H]$ and $E[\boldsymbol{H}_b(x)(\boldsymbol{H}_b(x))^H]$ can be obtained as

$$E[\boldsymbol{H}_a(x)(\boldsymbol{H}_a(x))^H]|_{(m,n)} = \sum_{i=0}^{L-x-\max(m,n)} \boldsymbol{C}_h(x+m+i, x+n+i) \tag{52}$$

$$E[\boldsymbol{H}_b(x)(\boldsymbol{H}_b(x))^H]|_{(m,n)} = \sum_{i=0}^{\min(m,n)-1} \boldsymbol{C}_h(m-i, n-i). \tag{53}$$

Substituting (52), (53) and (51) into (49), we finally obtain the interference plus extra noise power Ξ caused by the OLA method which varies with M_d for a fixed k_{ft}. We obtain the optimal M_d that minimizes Ξ as

$$M_d^* = \arg\min_{M_d}\{\Xi(M_d)\} \tag{54}$$

which can be numerically solved easily.

VI. Simulation Results and Discussions

We use the simulation parameters as specified in [2]: $N = 128$, $N_{\mathrm{pre}} = 5$, $N_{\mathrm{suf}} = 32$, $N_g = 37$, carrier frequencies $f_1 = 3432$ MHz, $f_2 = 3960$ MHz, $f_3 = 4488$ MHz, the sub-carrier spacing $1/T = 4.125$ MHz, and preamble pattern 1.[7] The normalized OFO v is set to 0.02. The channel model CM-2 with $\Omega_0 = 1$, $L_h = 6$ and $K = 6$ is adopted. $p(t)$ is a spectral raised cosine pulse with a filter span of $[-5T_s, 5T_s]$ and $t_0 = 5T_s$ unless mentioned otherwise. We define SNR as the ratio of the channel input signal power to the receive filter output noise power. The parameters of the synchronization method used are $\mathcal{M}_{\mathrm{SD}} = 0.5N\sigma^2$, $\Delta = 8$, $\Delta_1 = 1$, $W_1 = 165$, $W_2 = 32$, $W_3 = 32$, and $H_q = 2$.

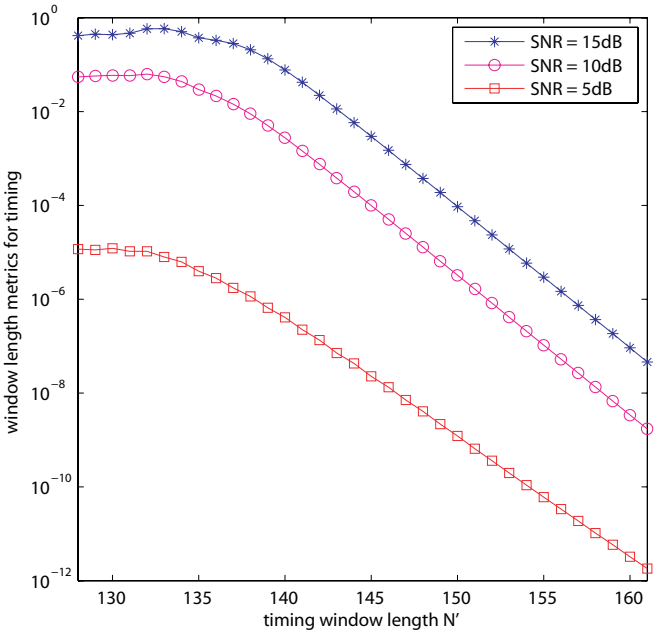

Fig. 2. The timing correlation window length design metric.

It should be pointed out that the proposed sync detection is based on $\Delta = 8$ times smaller sampling frequency than that of the conventional approach ($\Delta = 1$), and hence it requires only about $1/\Delta = 1/8$ of the complexity associated with the conventional sync detection approach. Note that the sync detection and coarse timing estimation performances based on $\Delta = 8$ are almost the same as those based on $\Delta = 1$ (see [18] for details).

Fig. 2 shows the proposed optimization metric of the timing correlation window length. The best timing correlation window length is $N_t = 130$ for SNR = 5 dB and $N_t = 132$ for SNRs = 10 and 15 dB. The metric differences are very small for $128 \leq N_t \leq 136$, but become significant as N_t increases further. The design results are almost insensitive to SNR values and we choose $N_t = 132$ in our simulation. The simulation results for the mean and the variance of the fine timing estimation obtained with $\eta = 0$ and several different window lengths are plotted in Fig. 3. The mean of the timing offset estimate depends on the correlation window length which can be ascribed to the different energy captures of different window sizes. The timing offset variances of different window sizes match very well with our design metric in Fig. 2. Also shown in Fig. 3 are the mean timing offsets obtained with different spans ($2t_0$ seconds or $1+(2t_0/T_s)$ taps) of the raised-cosine pulse-shape. We observe that the proposed fine timing estimator with $\eta = 0$ and the chosen window length $N_t = 132$

[7] Our method can also be applied to other preamble patterns.

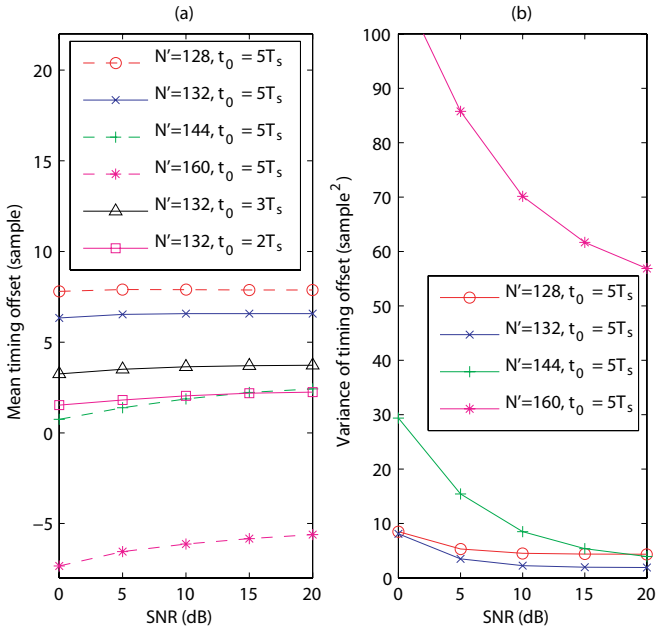

Fig. 3. The simulation results of the fine timing offset estimation with $\eta = 0$.

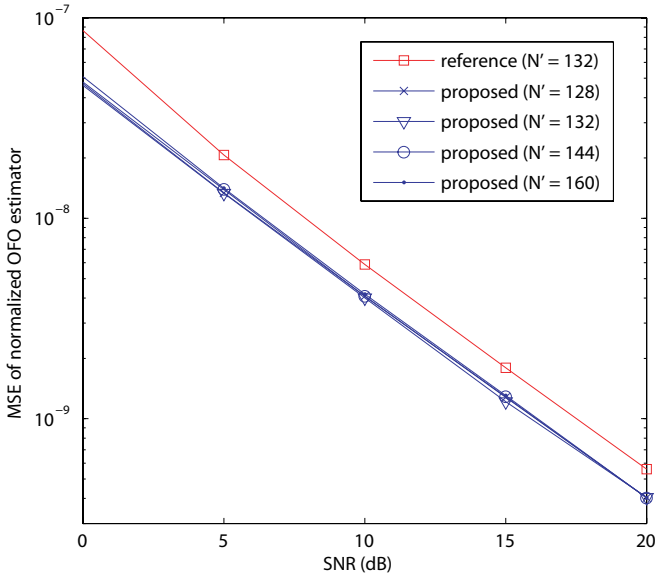

Fig. 4. The simulation results of the OFO estimation.

(see the curves with solid line in the figure) gives the mean timing offset (in samples) between (t_0/T_s) and $2 + (t_0/T_s)$ for SNRs of practical interest.

The OFO estimation[8] MSE results are given in Fig. 4. Both BLUE variance and MSE results are quite insensitive to different correlation window lengths. It can be seen from Fig. 4 that different window lengths give virtually the same MSE performance. Since using a smaller length requires smaller complexity, a good design choice is to use the best timing estimator correlation window length for the OFO estimator window length as well, i.e., $(N_f = N_t = 132)$. We also present the performance of a conventional estimator as a reference which is obtained by correlating adjacent OFDM symbols and averaging on each band. For the reference method, the estimated CFOs on the three bands are converted to OFO estimates (see (4)) and averaged to get an OFO estimate. It can be seen that the proposed OFO estimators outperform the reference estimator by nearly 2dB SNR advantage.

[8]The plots of the BLUE variances versus correlation window lengths and the corresponding discussion are skipped due to the space limitation (see [18] for details).

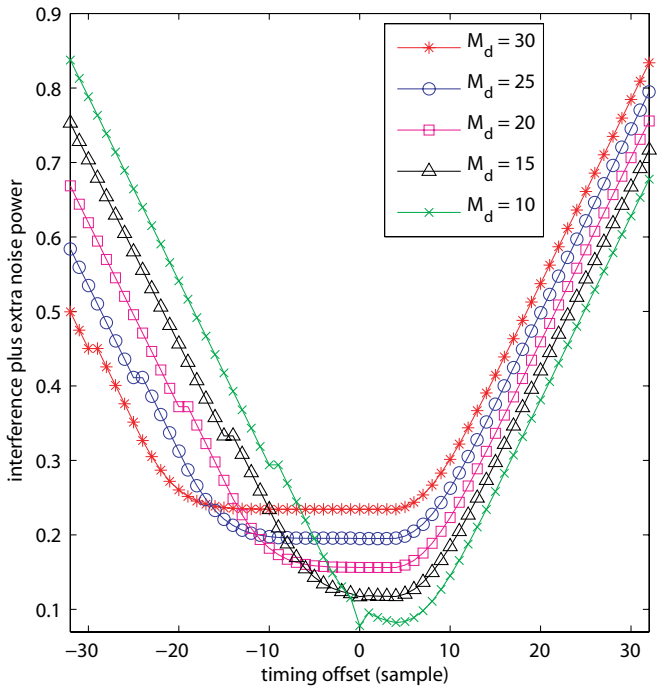

Fig. 5. The effects of timing offset and data OLA length M_d.

Fig. 5 presents the average interference plus extra noise power Ξ for several OLA lengths (M_d) and timing offsets. Ξ increases significantly when the timing offset lies outside a certain range $[a, b]$, e.g., $a = -8, b = 5$ for $M_d = 20$, and this range increases with M_d but b is observed to be fixed around t_0/T_s. For a particular M_d, the timing offset should be within the corresponding range $[a, b]$ in order to minimize the interference plus extra noise power. This range is similar to the ISI-free timing offset range in CP-based OFDM systems but there are two differences. First, in CP-based systems the above timing offset range is $[-N_g + L - 1, 0]$ and positive timing offsets definitely introduce interference, while in ZP OFDM systems the above timing offset range includes some positive timing offsets. Second, for a timing offset within the corresponding best timing offset range, there is neither interference nor extra noise for CP-based systems but there is always extra noise and possibly interference for ZP systems. The timing adjustment parameter η should be chosen such that the timing offset is most of the time within the above range $[a, b]$. Based on our observations in Fig. 3 and Fig. 5, our suggestion is to set η approximately equal to $\lceil \sigma_t + (t_0/T_s) \rceil$ where σ_t is the standard deviation of the fine timing estimator. We set $\eta = 10$ in our simulation with $t_0/T_s = 5$.

In Fig. 6, we present the channel estimation MSE given in (44) versus the channel estimation window length L' for different values of the OLA length M_p at SNR of 10 dB. For our considered channel, the best parameter setting for the CIR estimation under perfect synchronization is $([L']^*_{\text{perfect}} =$

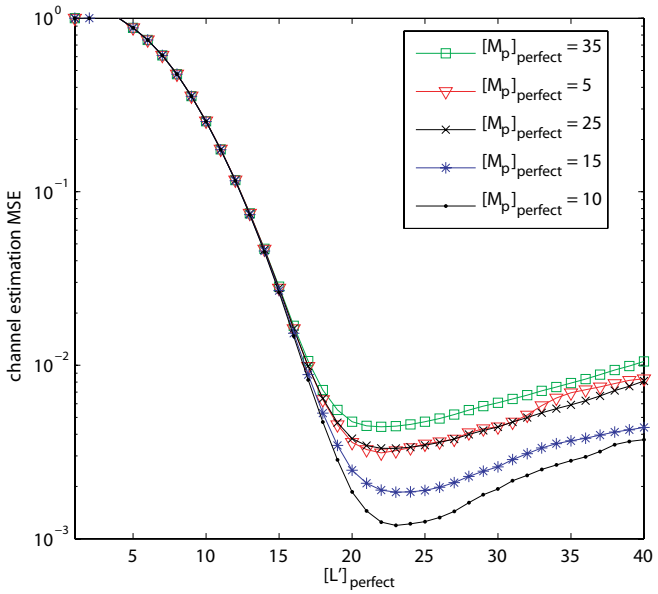

Fig. 6. The effects of CIR estimation length $[L']_{\text{perfect}}$ and preamble OLA length $[M_p]_{\text{perfect}}$ on the channel estimation MSE (SNR = 10dB) under perfect synchronization.

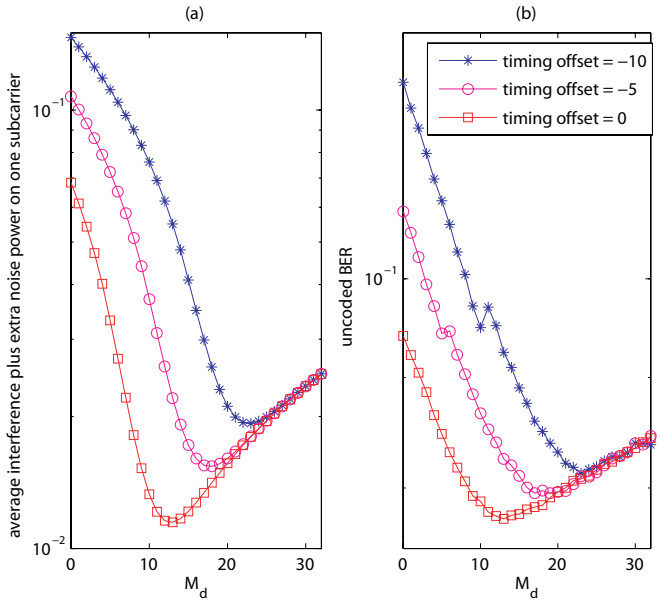

Fig. 7. The effect of data OLA length M_d (SNR = 10 dB). (a) Proposed design metric for M_d (b) The uncoded BER performance versus M_d.

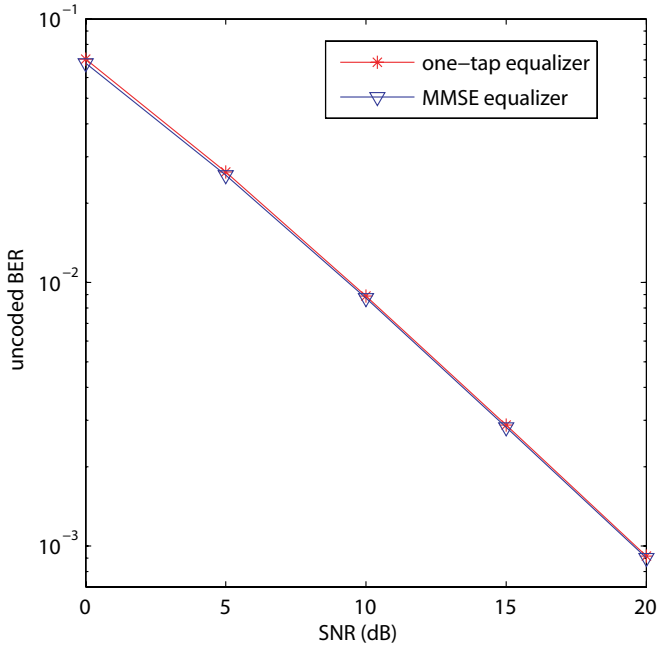

Fig. 8. The uncoded BER performance of the UWB systems using one-tap equalizer and MMSE equalizer with $M_d = 20$, assuming perfect timing, OFO and channel estimations.

23, $[M_p]^*_{\text{perfect}} = 10$). The MSE performance degradation due to the use of a smaller L' than $[L']^*_{\text{perfect}}$ is more significant than that due to the use of a larger L'. When taking into account the random timing offset $\Delta_k = k_{\text{ft}} - k_{\text{ref}}$, the L' should be chosen larger than $[L']^*_{\text{perfect}}$ so that most of the time the CIR estimation window contains the first $[L']^*_{\text{perfect}}$ actual CIR taps. M_p should also be increased accordingly. A good design is to set $L' = [L']^*_{\text{perfect}} + \lceil \sigma_t - E[\Delta_k] \rceil + 2$ and $M_p = [M_p]^*_{\text{perfect}} + \lceil \sigma_t - E[\Delta_k] \rceil + 2$. With $t_0/T_s = 5$, $N_t = 132$, and $\eta = 10$, we have $\lceil \sigma_t - E[\Delta_k] \rceil \simeq 5$ and hence a good choice is $L' = 30$ and $M_p = 17$. At SNR of 15 dB [9], we obtain $[L']^*_{\text{perfect}} = 25$ and $[M_p]^*_{\text{perfect}} = 12$, and hence $L' = 32$ and $M_p = 19$. Since $[L']_{\text{perfect}}$ and $[M_p]_{\text{perfect}}$ are quite insensitive to the SNR, we can use the same L' and M_p for different SNRs in our design.

Fig. 7(a) presents the plot of Ξ/N versus M_d at SNR $= 10$ dB with different fixed timing offset values[10] of 0, -5 and -10 samples, respectively. We observe that with perfect timing the best M_d is 13, while with a timing offset Δ_k (a negative number due to the timing advancement) the best M_d is $13 - \Delta_k$. In Fig. 7(b) we present the corresponding uncoded BER simulation results for the QPSK modulated signals with one-tap frequency-domain equalization. The BER curves are consistent with the interference plus extra noise power curves in Fig. 7(a). Note that choosing a larger value of M_d is more robust to random timing offsets. Our suggestion is to set M_d a few samples (say 2) larger than the best M_d value corresponding to a timing offset around $\lceil E[\Delta_k] - \sigma_t \rceil$. With $t_0/T_s = 5$, $N_t = 132$, and $\eta = 10$, this timing offset would be around -5 and hence a good choice for M_d is 20, which is close to $M_p = 17$, and hence we may set $M_p = M_d = 20$ for simplicity.

[9]The corresponding plots are omitted due to the space limitation.

[10]We only consider non-positive timing offsets since the timing adjustment yields negative timing offset most of the time.

In Fig. 8, we present the uncoded BER performances for the UWB systems using one-tap equalizer and MMSE equalizer assuming perfect timing, OFO and channel estimations. The BER advantage of the MMSE equalizer is marginal, indicating the one-tap equalizer as a preferred choice due to its low complexity advantage.

Finally, Fig. 9 and Fig. 10 present the uncoded BER performance. The "reference" in the figures represents the system performance obtained by using conventional methods and parameters, i.e. correlation-based timing estimator with $N_t = 160$, the conventional CFO estimator mentioned before

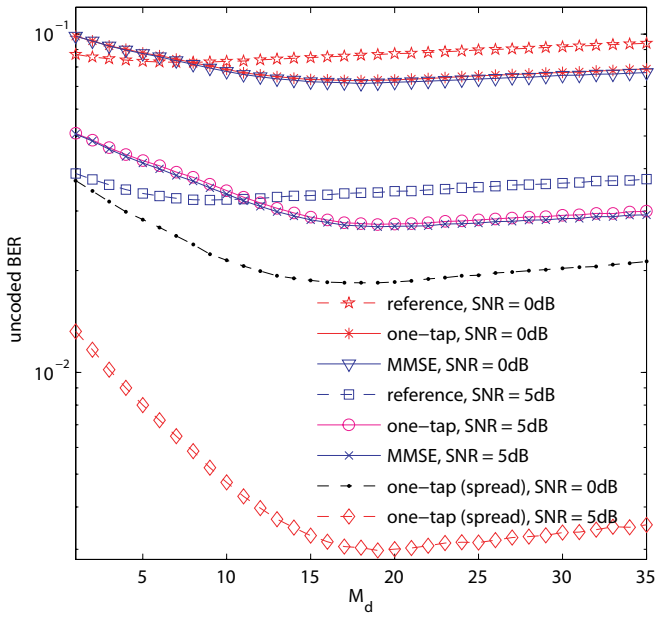

Fig. 9. The uncoded BER performance of the proposed and reference methods with $N_t = N_f = 132$, $L' = 28$, $\eta = 10$ versus the OLA length ($M_d = M_p$) when SNRs = 0, 5 dB.

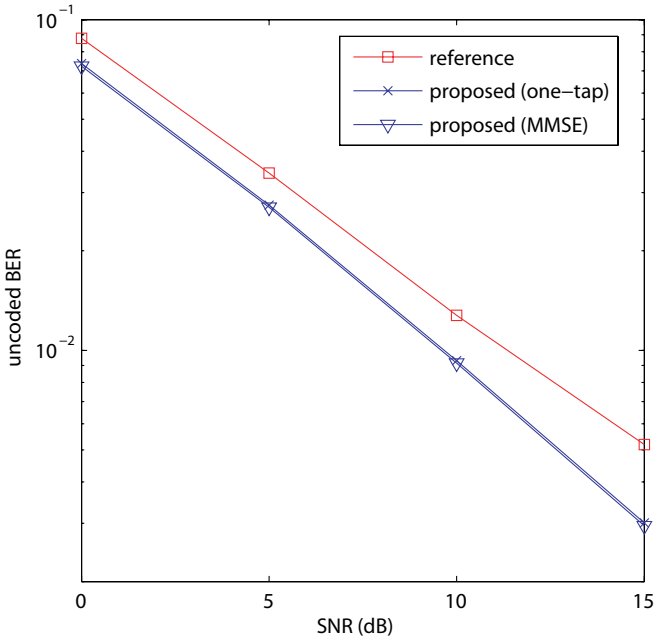

Fig. 10. The uncoded BER performance of the proposed and reference methods with $N_t = N_f = 132$, $L' = 28$, $\eta = 10$, and $M_d = M_p = 20$.

for Fig. 4, frequency domain least-square channel estimator, and one-tap ZF frequency-domain equalizer. The proposed method uses $N_t = N_f = 132$, and $L' = 28$.

In Fig. 9, we present the uncoded BER performance versus M_d $(= M_p)$ at SNR = 0, 5 dB (the performance plots for SNR = 10, 15 dB are skipped due to space limitation; see [18] for details). Compared with the reference method, our proposed methods obtain nearly 2 dB SNR advantage. We observe that the optimum values of M_d slightly vary with different SNR values and our design of $M_p = M_d = 20$ gives approximately the best result across the SNRs of interest. And the performance difference between the one-tap ZF equalizer and the MMSE equalizer is small. The BER curve for the time-frequency spread data is shown as "(spread)" in Fig. 9. We observe that at the cost of data rate reduction, the spreading improves the error performance significantly.

In Fig. 10, we present the uncoded BER performance versus SNR. We use M_d $(= M_p)$ $= 20$ for both proposed and reference methods. The proposed method gives about 2 dB SNR advantage at uncoded BER of 10^{-2}. The BER performance advantage of the proposed method becomes more obvious at higher SNR, which may be ascribed to its better synchronization performance and the fact that the BER performance is dominated by synchronization errors at higher SNR and by the noise at lower SNR.

VII. Conclusions

We have presented low complexity synchronization, channel estimation and equalization methods for MB-OFDM based UWB systems by utilizing the distinctive features of MB-OFDM systems. We have derived the probability density functions (pdfs) of the UWB channel path delays and using these pdfs we present how to optimize the synchronization, channel estimation and equalization methods. The timing estimation performance is more sensitive to the correlation window length than the frequency offset estimation. Hence, although the best correlation window lengths for timing and frequency offset estimation are not the same, we may use the same correlation window length designed for the timing estimation when performing both tasks. The best overlap-add window lengths for preamble and data are observed to be approximately the same, and the use of the overlap-add length larger than the best value gives a more robust performance than the use of a smaller length. The MMSE equalizer for the ZF-OFDM systems is no longer a one-tap frequency-domain equalizer, but the latter gives almost the same performance as the former, and hence is a better choice for practical systems. The simulation results corroborate the effectiveness of our proposed synchronization, channel estimation and equalization methods and corresponding optimization criteria.

Appendix

In (33), we find that the matrix $\boldsymbol{\Psi} \triangleq \left(\boldsymbol{H}_q \boldsymbol{C}_{\tilde{s}} \boldsymbol{H}_q^H + \boldsymbol{C}_n\right)$, which needs to be inverted, is a patterned matrix with the form $\boldsymbol{\Psi} = \boldsymbol{D} + \sigma^2 \sum_{k=1}^{M_d} \boldsymbol{f}_k \boldsymbol{f}_k^H$, where $\boldsymbol{D} = \boldsymbol{H}_q \boldsymbol{C}_{\tilde{s}} \boldsymbol{H}_q^H + \sigma^2 \boldsymbol{I}_N$ is a nonsingular diagonal matrix, $\{\boldsymbol{f}_k\}$ are $N \times 1$ DFT vectors. Applying a similar approach from Theorem 8.3.3 in [19], the inverse of Ψ can be simplified by

$$\boldsymbol{\Psi}^{-1} = \left(\boldsymbol{H}_q \boldsymbol{C}_{\tilde{s}} \boldsymbol{H}_q^H + \sigma^2 \boldsymbol{I}_N\right)^{-1} + \sum_{k=1}^{M_d} \tilde{\gamma}_k \boldsymbol{D}^{-1} \boldsymbol{f}_k (\boldsymbol{D}^{-1} \boldsymbol{f}_k)^H \tag{55}$$

where $\tilde{\gamma}_k = -\sigma^2/(1 + \sigma^2 \boldsymbol{f}_k^T \boldsymbol{D}^{-1} \boldsymbol{f}_k^*)$. By applying (55) we avoid the non-diagonal matrix inverse and reduce the complexity of the MMSE Equalizer.

The MMSE equalizer for the system with the data spreading needs the inverse of the matrix $\boldsymbol{V}$ defined in (35), which is

given by [19]

$$\{\boldsymbol{V}^{-1}\}_{11} = [\boldsymbol{V}_{11} - \boldsymbol{V}_{12}\boldsymbol{V}_{22}^{-1}\boldsymbol{V}_{21}]^{-1} \quad (56)$$

$$\{\boldsymbol{V}^{-1}\}_{12} = -\boldsymbol{V}_{11}^{-1}\boldsymbol{V}_{12}[\boldsymbol{V}_{22} - \boldsymbol{V}_{21}\boldsymbol{V}_{11}^{-1}\boldsymbol{V}_{12}]^{-1} \quad (57)$$

$$\{\boldsymbol{V}^{-1}\}_{21} = -\boldsymbol{V}_{22}^{-1}\boldsymbol{V}_{21}[\boldsymbol{V}_{11} - \boldsymbol{V}_{12}\boldsymbol{V}_{22}^{-1}\boldsymbol{V}_{21}]^{-1} \quad (58)$$

$$\{\boldsymbol{V}^{-1}\}_{22} = [\boldsymbol{V}_{22} - \boldsymbol{V}_{21}\boldsymbol{V}_{11}^{-1}\boldsymbol{V}_{12}]^{-1} \quad (59)$$

where $\boldsymbol{V}_{11} \triangleq \boldsymbol{H}_{l_\xi}\boldsymbol{C}_{\tilde{s}}\boldsymbol{H}_{l_\xi}^H + \boldsymbol{C}_n$, $\boldsymbol{V}_{12} \triangleq \boldsymbol{H}_{l_\xi}\boldsymbol{C}_{\tilde{s}}\boldsymbol{H}_{n_\xi}^H$, $\boldsymbol{V}_{21} \triangleq \boldsymbol{H}_{n_\xi}\boldsymbol{C}_{\tilde{s}}\boldsymbol{H}_{l_\xi}^H$ and $\boldsymbol{V}_{22} \triangleq \boldsymbol{H}_{n_\xi}\boldsymbol{C}_{\tilde{s}}\boldsymbol{H}_{n_\xi}^H + \boldsymbol{C}_n$. $\boldsymbol{V}_{12}$ and $\boldsymbol{V}_{21}$ are diagonal matrices, and $\boldsymbol{V}_{11}$ and $\boldsymbol{V}_{22}$ have the same pattern as $\boldsymbol{\Psi}$. Hence, the computation of the inverse can be simplified using the method we proposed for $\boldsymbol{\Psi}^{-1}$.

REFERENCES

[1] A. Batra, J. Balakrishnan, G. Aiello, J. Foerster, and A. Dabak, "Design of a multiband OFDM system for realistic UWB channel environments," *IEEE Trans. Microwave Theory Tech.*, vol. 52, no. 9, pp. 2123–2138, Sept. 2004.

[2] Multi-band OFDM physical layer proposal for IEEE 802.15 Task Group 3a, IEEE Std., Mar. 2004.

[3] High rate ultra wideband PHY and MAC standard, ECMA Std., 2005.

[4] D. Dardari, V. Tralli, and A. Vaccari, "A theoretical characterization of nonlinear distortion effects in OFDM systems," *IEEE Trans. Commun.*, vol. 48, no. 10, pp. 1755–1764, Oct. 2000.

[5] T. Pollet, M. Van Bladel, and M. Moeneclaey, "BER sensitivity of OFDM systems to carrier frequency offset and Wiener phase noise," *IEEE Trans. Commun.*, pp. 191–193, Feb.-Mar.-Apr. 1995.

[6] H. Steendam and M. Moeneclaey, "Synchronization sensitivity of multi-carrier systems," *European Commun.*, ETT special issue on multi-carrier spread spectrum, vol. 52, pp. 834–844, May 2004.

[7] Y. Zhou, A. Karsilayan, and E. Serpedin, "Sensitivity of multiband ZP-OFDM ultra-wide-band and receivers to synchronization errors," *IEEE Trans. Signal Processing*, vol. 55, no. 2, pp. 729–734, Jan. 2007.

[8] P. Moose, "A technique for orthogonal frequency division multiplexing frequency offset correction," *IEEE Trans. Commun.*, vol. 42, no. 10, pp. 2908–2914, Oct. 1994.

[9] H. Minn and P. Tarasak, "Improved maximum likelihood frequency offset estimation based on likelihood metric design," *IEEE Trans. Signal Processing*, vol. 54, no. 6, pp. 2076–2086, June 2006.

[10] H. Minn, V. Bhargava, and K. Letaief, "A robust timing and frequency synchronization for OFDM systems," *IEEE Trans. Wireless Commun.*, vol. 2, no. 4, pp. 822–839, July 2003.

[11] H. Minn, V. K. Bhargava, and K. B. Letaief, "A combined timing and frequency synchronization and channel estimation for OFDM," *IEEE Trans. Commun.*, vol. 54, no. 3, pp. 416–422, Mar. 2006.

[12] Y. Li, T. Jacobs, and H. Minn, "Frequency offset estimation for MB-OFDM-based UWB systems," in *Proc. IEEE ICC*, vol. 10, June 2006, pp. 4729–4734.

[13] C. W. Yak, Z. ling Lei, S. Chattong, and T. T. Tjhung, "Timing synchronization and frequency offset estimation for ultra-wideband (UWB) multiband OFDM systems," in *Proc. IEEE Intl. Symp. on Personal, Indoor and Mobile Radio Commun.*, vol. 1, 11-14 Sept. 2005, pp. 471–475.

[14] C. Berger, S. Zhou, Z. Tian, and P. Willett, "Precise Timing for Multiband OFDM in a UWB System," in *Proc. IEEE International Conference on Ultra-Wideband*, Sept. 2006, pp. 269–274.

[15] S. Traverso, I. Fijalkow, and C. Lereau, "Improved equalization for UWB multiband OFDM," in *Proc. Information and Communication Technologies 2006 (ICTTA '06)*, vol. 2, Apr. 2006, pp. 2634–2638.

[16] B. Muquet, Z. Wang, G. Giannakis, M. de Courville, and P. Duhamel, "Cyclic prefixing or zero padding for wireless multicarrier transmissions?" *IEEE Trans. Commun.*, vol. 50, no. 12, pp. 2136–2148, Dec. 2002.

[17] A. Molisch, J. Foerster, and M. Pendergrass, "Channel models for ultrawideband personal area networks," *IEEE Wireless Commun.*, vol. 10, no. 6, pp. 14–21, Dec. 2003.

[18] T. Jacobs, Y. Li, H. Minn, and R. Rajatheva, "Synchronization in MB-OFDM-based UWB systems," in *Proc. IEEE ICC*, June 2007, pp. 1071–1076.

[19] F. Graybill, *Matrices with Applications in Statistics*. Wadsworth Publishing, 1983.

Yinghui Li (S'05) received the B.E. and M.S. degrees in Electrical Engineering from the Nanjing University of Aeronautics and Astronautics, Nanjing, China, in 2000 and 2003, and the Ph.D. degree in Electrical Engineering from the University of Texas at Dallas in 2007. From 2004 to 2007, she was a Research Assistant with the Information and Communications Systems Laboratory at UTD. Since 2008, she has been with LitePoint Inc, CA, USA. Her research interests include signal processing algorithms and training signal designs for broadband wireless communications.

Hlaing Minn (S'99-M'01-SM'07) received his B.E. degree in Electronics from Yangon Institute of Technology, Yangon, Myanmar, in 1995, M.Eng. degree in Telecommunications from Asian Institute of Technology (AIT), Thailand, in 1997 and Ph.D. degree in Electrical Engineering from the University of Victoria, Victoria, BC, Canada, in 2001.

He was with the Telecommunications Program in AIT as a laboratory supervisor during 1998. He was a research assistant from 1999 to 2001 and a post-doctoral research fellow during 2002 in the Department of Electrical and Computer Engineering at the University of Victoria. He has been with the University of Texas at Dallas, USA, since 2002, and currently he is an Associate Professor. His research interests include wireless communications, statistical signal processing, error control, detection, estimation, synchronization, signal design, cross-layer design, and cognitive radios. He is an Editor for the IEEE TRANSACTIONS ON COMMUNICATIONS, and the JOURNAL OF COMMUNICATIONS AND NETWORKS.

Nandana Rajatheva received the B.Sc. degree in Electronic and Telecommunication Engineering with first class honors from the university of Moratuwa, Moratuwa, Sri Lanka, in 1987, and the M.Sc., Ph.D. degrees from the University of Manitoba, Winnipeg, MB, Canada in 1991 and 1995 respectively. Currently he is an Associate Professor in the Telecommunications Field of Study, School of Engineeing and Technology, Asian Institute of Technology (AIT), Thailand. He was with the University of Moratuwa, Sri Lanka before joining AIT where he was promoted to Professor in Electronic & Telecommunication Engineering in June 2003. From May 1996 to Dec.2001, he was with TC-SAT as an Associate Professor. His research interests include wireless communications with applications in OFDM and MIMO systems, signal processing and coding techniques in communications.